Mapping Mineralogical and structural relationships with satellite-borne ASTER and airborne geophysics at Broken Hill

R.D.Hewson*
CSIRO – CEM, Australia
Rob.Hewson@csiro.au

A.Mah
ERMapper, Australia
Abdullah.Mah@ermapper.com.au

M.Dunne
ERMapper, Australia
Mike.Dunne@ermapper.com.au

T.J.Cudahy
CSIRO-CEM, Australia
Thomas.Cudahy@csiro.au

SUMMARY

The recent availability of 14 band multi-spectral and 15 metre DEM data from the satellite borne ASTER (Advanced Spaceborne Thermal Emission Reflection Radiometer) instrument has introduced new possibilities for geological mapping and integration with traditional geophysical data sets. Calibrated radiance at the sensor data and atmospheric corrected ASTER products, such as surface reflectance and emissivity imagery, have been made available by NASA/USGS and the Japanese agency, ERSDAC. ASTER radiance data measures five bands at 30 metre resolution, within the short-wave infrared 2.1 to 2.5 μm wavelength region, and also five bands at 90 metre resolution within the 8 to 12 μm thermal infrared region. This compares with only one band as measured by Landsat TM for each of these regions. An investigation into the capabilities of ASTER and strategies for its integration with geophysical data (using ER Mapper) was undertaken at Broken Hill, given its high spatial geological control and extensive airborne geophysical data sets. Mineral (group) maps derived from multi-scene ASTER data, collected over the Broken Hill Block, proved useful for discriminating stratigraphic units, regolith and areas of alteration. In particular ASTER imagery highlighted several sericite-rich as well as quartz-rich colluvial regolith. Variations in ASTER's derived AlOH mineral spectral signatures correlated with higher potassium radiometric responses and indicated a change in the muscovite chemistry, possibly due to retrograde metamorphic alteration. However structural features associated with retrograde shear zones were identified most clearly using aeromagnetics. Overall ASTER data products provided complementary mineralogical information to the structural interpretation afforded by geophysical data sets.

INTRODUCTION

The availability of multi-spectral data from the satellite-borne ASTER sensor, launched in December 1999 has signalled the start of a new era in large scale mapping of the Earth's surface composition. Laboratory spectroscopy studies of various mineralogies have indicated the potential to identify and discriminate mineralogy from their diagnostic visible, near infrared, shortwave infrared and thermal infrared spectral signatures (Clark *et al*, 1990; Salisbury *et al*., 1992). The ASTER sensor now offers the opportunity of mapping within a 60 x 60 kilometre scene area from three 15 metre pixel resolution visible-near-infrared (VNIR) channels, six 30 metre pixel resolution shortwave infrared (SWIR) channels and five 90 metre pixel resolution thermal infrared (TIR) channels (Fujisada *et al*., 1998) (Table 1). ASTER radiance data includes five bands within the short-wave infrared wavelength region between 2.1 to 2.5 μm and also five bands within the 8 to 12 μm thermal infrared region. This compares with only one band as measured by Landsat TM for each of these regions. The increased spectral capability of ASTER to measure radiance within the short-wave infrared region (SWIR) therefore has considerable potential advantage over Landsat TM for discriminating spectral features (Figure 1). The ASTER instrument, developed and operated by the Japanese agency, ERSDAC, is on board the US Terra satellite and forms part of the NASA EOS mission, collecting environmental and geological surface information from 2000 to 2005. An extensive range of data products for ASTER scenes of 60 by 60 kilometres in size are now available via ERSDAC and NASA-USGS web sites, including calibrated radiance to the sensor, surface reflectance, surface emissivity imagery, surface kinetic temperature and digital elevation model data
(http://asterweb.jpl.nasa.gov/gettingdata/;
http://www.ersdac.or.jp/eng/index.E.html).

Comparisons between various image products processed from ASTER and airborne visible-shortwave and thermal infrared survey data sets from the Mt Fitton CSIRO test site, situated in the northern Flinders Ranges of South Australia, have validated the application of ASTER Level 1B data for geological and alteration mapping (Hewson *et al*., 2001). Detailed geological mapping from two mosaiced ASTER scenes have also proved successful in the Bangemall Basin of Western Australia (Hewson *et al*., 2002). This study further investigates the geological and alteration mapping potential of mosaicing ASTER imagery over a large area of the Broken Hill Block in conjunction with detailed airborne geophysical data.

Broken Hill

The world class Broken Hill Pb-Zn-Ag orebody within the Curnamona Province of NSW-SA, is associated with an extensive range of high grade metamorphic rocks (Stevens *et al*., 1988). Various alteration phases have occurred and the relationship of their association with the Broken Hill Orebody is under discussion. Studies of regional retrograde metamorphism of high grade Broken Hill units, studied previously by Corbett and Phillips (1981), have indicated the presence of retrograde alteration minerals such as chlorite and

low grade variations of muscovite/sericite. In particular Broken Hill pelites have been shown to contain less K_2O and FeO and higher Na/(Na + K) with increasing retrogression (Corbett and Phillips, 1981). This study attempted to investigate the association of potassium content, using airborne radiometrics, and sericite/muscovite with remote sensing techniques.

METHOD AND RESULTS

Airborne geophysics

Detailed Broken Hill geophysical data (magnetics and radiometrics), acquired as part of the NSW's DMR Discovery 2000 and Geoscience Australia BHEI programmes were processed using ER Mapper (http://www.ermapper.com/). This data was acquired at 100-metre flight line spacing in east-west flight lines across the Broken Hill Block. In particular, two data sets (P617 and P633) were calibrated, mosaiced and registered to Datum WGS84, Projection zone SUTM54. Radiometric data K, Th and U were displayed in an enhanced ternary RGB color composite (Figure 2a). The structure and lineaments associated with the retrograde shear zones were highlighted using an Automatic Gain Control filter of 9 by 9 matrix applied to the aeromagnetics data. Draping the radiometrics Ternary image over the AGC filtered magnetics combined both the surface chemistry and the subsurface structures (Figure 2b).

ASTER imagery

Level 1B ASTER imagery was ordered via the Eros Data Gateway (EDG) of NASA's ASTER web site (listed above) and calibrated to $W/m^2/sr/\mu m$ radiance at the sensor using ER Mapper. The gap in the Broken Hill imagery apparent in Figures 2c - 2f (54000E, 6500000N) remains to be acquired by the ASTER sensor. However such gaps are envisaged to be acquired soon given the high priority assigned by ERSDAC/NASA of collecting complete cloud free global coverage by 2004. Variations and boundaries between ASTER scenes acquired on different days are also apparent in some areas partly due to variable atmospheric water concentrations and are in the process of being addressed. Despite these issues, useful images from the ASTER data were produced to represent sericite abundance using the ASTER SWIR band combination algorithm: (B5+B7)/B6, thresholded at 99%, highlighting the diagnostic spectral absorption feature for AlOH/sericite, centred at approximately ASTER band 6 at 2.20 μm (Figure 2c). An RGB colour composite of B5/B6; B7/B6; B7/B5 (threshold 99%) was produced for all ASTER scenes to represent possible shifts in the wavelength of the AlOH absorption feature which has previously been shown to indicate changes in the white mica chemistry due to loss of Al and substitution of Si, Mg or Fe (Duke, 1994) (Figure 2d).

In a similar way, the Broken Hill ASTER imagery was processed for band ratio B13/B10 using the NASA supplied TIR atmosphere corrected surface emissivity product (Level 2) to highlight quartz content (Figure 2e). This image particularly highlights the quartz associated with regolith colluvial/alluvial cover.

The relationship of the ASTER derived AlOH/white mica composition with chemistry was further examined by integrating it with the image of the higher potassium levels (thresholded to 130 and median filtered at n=11) (Figure 2f). It appears that there is an association of the higher potassium content with the longer wavelength, more phengitic white mica indicated by the higher ASTER B5/B6 ratio, relative to B7/B6, highlighted by the red areas (*i.e.* 530000E, 6500000N, Figures 2d & 2f). Earlier laboratory studies by Scott and Yang (1997) have indicated the substitution of Na for K is associated with paragonite that displays a shorter wavelength absorption feature. Although some areas (*ie* 550000E, 6500000N) do not have a clear correlation between high B5/B6 with high potassium, issues of across scene calibration, image thresholding and water vapour variations require further investigation. However it appears that decreasing retrograde metamorphic alteration (*i.e.* K_2O rich) to be generally highlighted by those white micas with higher potassium radio-element content and a longer ASTER wavelength AlOH absorption feature.

CONCLUSIONS AND RECOMMENDATIONS

ASTER imagery at Broken Hill indicated that it could provide detailed geological mapping, providing more discrimination regarding about mineral (group) content and possible composition. Integration of airborne geophysics assists in the interpretation of structural features and complements surface chemistry and remote sensing imagery. In particular the comparison of radiometrics with ASTER derived AlOH imagery appears to correlate more phengitic micaceous units with higher potassium concentrations, possibly associated with decreased retrograde metamorphism. Further field investigations are required and currently being undertaken to confirm these results.

ACKNOWLEDGMENTS

Airborne geophysical data used in this study was gratefully obtained from Geoscience Australia and the NSW DMR, acquired as part of the Broken Hill Exploration Initiative and Discovery 2000 programmes. Support and assistance from South Australia's Department of Primary Industries and Resources (PIRSA) for the acquisition and calibration of ASTER data over the Curnamona Province is also gratefully acknowledged.

REFERENCES

Clark, R.N., King, T.V.V., Klejwa, M., and Swayze, G.A., 1990. High spectral resolution reflectance spectroscopy of minerals*: Journal* Geophysical Research: 95, B8, 12653-12680.

Corbet, G.J., and Phillips, G.N., 1981. Regional retrograde metamorphism of a high-grade terrain: the Willyama Complex, Broken Hill, Australia: Lithos, 14, 59- 73.

Duke, E.F., 1994. Near infrared spectra of muscovite. Tschermak substitution and metamorphic reaction process: Implications for remote sensing: Geology, 22, 201-219.

Fujisada, H., Sakuma, F., Ono, A., and Kudoh, M., 1998. Design and pre-flight performance of ASTER instrument

protoflight model: IEEE Transactions. Geoscience Remote Sensing, 36, 4, 1152-1160.

Hewson, R.D., Cudahy, T.J. , and Huntington, J.F., 2001. Geologic and alteration mapping at Mt Fitton, South Australia, using ASTER satellite-borne data: IEEE 2001 International Geoscience and remote sensing Symposium (IGARSS), 9-13 July.

Hewson, R., Koch, C., Buchanan, A., and Sanders, A., 2002. Detailed geological and regolith mapping in the Bangemall Basin, WA, using ASTER multi-spectral satellite-borne data: Eleventh Australasian Remote Sensing and Photogrammetric Conference, Brisbane, 2-5th September.

Salisbury, J.W. and D Aria, D.M., 1992. Emissivity of terrestrial materials in the 8-14 μm atmospheric window: Remote Sensing Environment, 42, 83-106.

Stevens B.P.J., Barnes R.G., Brown R.E., Stroud W.J.and Willis I.L., (1988): The Willyama Supergroup in the Broken Hill and Euriowie Blocks, New South Wales: Precambrian Research, 40, 297-327.

Scott, K.M. and Yang, K. 1997. Spectral reflectance studies of white micas: CSIRO Exploration and Mining Report 439R.

Windeler, D.S., 1993. Garnet-pyroxene alteration mapping in the Ludwig skarn (Yerington, Nevada) with Geoscan airborne multispectral data: Photogrammetric Engineering and Remote Sensing, 59, 8, 1277-1286.

Spectral Range	VNIR μm	SWIR μm	TIR μm
FWHM [Centre λ]	Band 1 0.52 – 0.60 [0.556]	Band 4 1.600 – 1.700 [1.656]	Band 10 8.125 – 8.475 [8.291]
	Band 2 0.63 – 0.69 [0.661]	Band 5 2.145 – 2.185 [2.167]	Band 11 8.475 – 8.825 [8.634]
	Band 3N 0.78 – 0.86 [0.807]	Band 6 2.185 – 2.225 [2.209]	Band 12 8.925 – 9.275 [9.075]
	Band 3B 0.78 – 0.86 [0.804] Backward looking	Band 7 2.235 – 2.285 [2.262]	Band 13 10.25 – 10.95 [10.657]
		Band 8 2.295 – 2.395 [2.336]	Band 14 10.95 – 11.65 [11.318]
		Band 9 2.360 – 2.430 [2.400]	
Ground Resolution (m)	15	30	90
Dynamic Range	8	8	12

Table 1 Spectral, spatial and image specifications of the ASTER sensor (Fujisada *et al*., 1998)

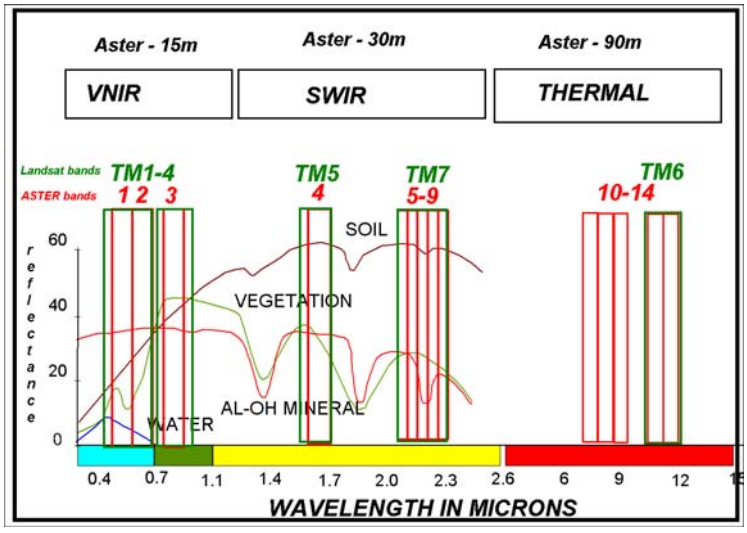

Figure 1 ASTER spectral bands (red) compared to Landsat TM bands (green) compared to spectral fetures of water, soil and green vegetation (Buchanan, pers. comm.)

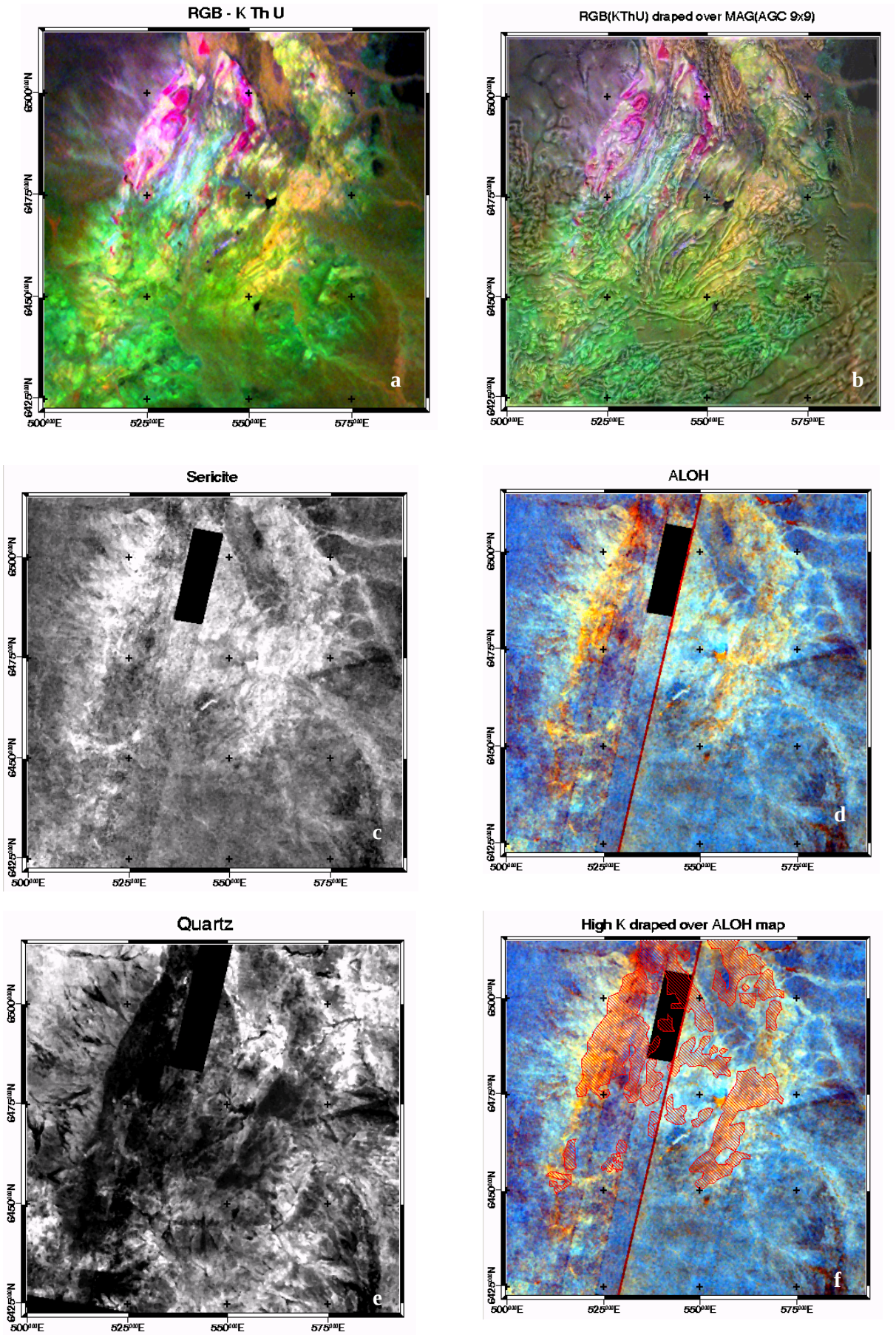

Figure 2 a) Ternary K Th U image of radiometric data; b) Ternary K Th U draped over AGC processed TMI; c) ASTER derived image of sericite content; d) ASTER derived AlOH (white mica) composition; e) ASTER derived quartz regolith; f) Thresholded K over AlOH composition.